Taylor & Francis
Taylor & Francis Group

Automatika

Journal for Control, Measurement, Electronics, Computing and Communications

ISSN: (Print) (Online) Journal homepage: www.tandfonline.com/journals/taut20

Frequency control scheme based on the CDM-PID controller for the hybrid microgrid system with stochastic renewable generators

M'hamed Helaimi, Hossam A. Gabbar, Rachid Taleb & Mohamed Regad

To cite this article: M'hamed Helaimi, Hossam A. Gabbar, Rachid Taleb & Mohamed Regad (2023) Frequency control scheme based on the CDM-PID controller for the hybrid microgrid system with stochastic renewable generators, Automatika, 64:3, 484-495, DOI: 10.1080/00051144.2023.2192380

To link to this article: https://doi.org/10.1080/00051144.2023.2192380

Published online: 29 Mar 2023.

AUTOMATIKA
2023, VOL. 64, NO. 3, 484–495
https://doi.org/10.1080/00051144.2023.2192380

REGULAR PAPER

OPEN ACCESS Check for updates

Frequency control scheme based on the CDM-PID controller for the hybrid microgrid system with stochastic renewable generators

M'hamed Helaimi[a], Hossam A. Gabbar[b], Rachid Taleb[a] and Mohamed Regad[a]

[a]Electrical Engineering Department, Laboratoire Génie Electrique et Energies Renouvelables (LGEER), Hassiba Benbouali University, Chlef, Algeria; [b]Faculty of Energy Systems and Nuclear Science, University of Ontario Institute of Technology (UOIT), Oshawa, Canada

ABSTRACT

In this paper, we introduce a Coefficient Diagram Method (CDM) to design a conventional PID controller. This controller is used to decrease the frequency fluctuations of a microgrid system composed of two renewable energy sources (WTG and STPG) and four controlled elements (UC, FESS, BESS and DEG). The method compares two characteristic polynomials of the same order:, the coefficients of the first polynomial are a function of microgrid parameters and the unknown gains of the PID controller. The second is called the target polynomial; its coefficients are calculated by choosing the stability indices and the equivalent time constant to satisfy the desired performances of the closed-loop system. Mathematically, the order of the polynomial controller determines the type of linear system of equations to solve: undetermined or overdetermined. In our application, the least squares method is used to find an approximate solution to the overdetermined system resulting from this comparison. Digital simulation is performed to test the performance of the microgrid controlled by the CDM-PID controller. The obtained results are compared with two recently published works where the parameters of the PID controllers are tuned by DE and chaotic PSO algorithms. The results show that the CDM-PID controller gives better performance.

ARTICLE HISTORY
Received 23 September 2020
Accepted 30 August 2021

KEYWORDS
Microgrid; PID controller; coefficient diagram method (CDM); least squares method; chaotic PSO-PID; DE-PID

1. Introduction

Nowadays, specialists attribute the increase in electrical energy demand to the economic and demographic growth that the world witnessed after the Second World War. This development has prompted specialists to use natural resources to produce electrical energy to reduce the consumption of combustible energy which pollutes the environment due to gas emissions. To satisfy the need for electrical energy in isolated sites, numerous microgrids have been installed around the world. These small-scale systems are designed to produce electrical energy to supply local buildings, islands and military bases during normal and emergency operating conditions. They are made up of 3 main units: production, storage and management. Generally, microgrids consist of hybrid renewable energy sources (solar panels, isolated or non-isolated wind turbines), energy storage systems or even generators. The storage devices (batteries, ultracapacitor, etc.) are coupled to microgrid systems to improve efficiency and reduce frequency fluctuations. The renewable nature of PVs and wind turbines depends on climatic conditions; this dependence can affect the quality of the produced energy and especially the frequency stability of the overall system. In the literature, much theoretical research recently published has implemented conventional PID controllers [1–9], fractional PID controllers [1], [3–5], [10], fuzzy logic controllers [11,12], neural networks [13,14] to decrease the frequency fluctuations of microgrid systems. Other researchers have proposed new structures of combined controllers (fractional order-multistage PD/(1+PI) controller [15], robust fuzzy cascade PD-PI controller [16], fuzzy-aided PID controller [17] type-II fuzzy PID controller [18], tilt fuzzy cascade (TDF(1+TI)) controller [19], fractional order-based type-II fuzzy controller [20]) to regulate the frequency of the microgrid under different uncertainties.

In practice, the PID controller has emerged in more than 90% of industrial applications especially in the control of output power and frequency in microgrid systems due to its extreme simplicity and the performances it can offer to the closed loop satisfying the desired specifications. In these systems, the most used methods to compute the PID gains are based on Genetic Algorithm GA, Differential Evolution DE, particle swarm optimization PSO, Bacteria foraging BF or Krill Herd KH algorithms [1], [3,4], [9], [21,22]. These methods require formulating the optimization problem by defining the objective function and choosing the parameters of the algorithm to be applied, which limits their use.

CONTACT Rachid Taleb r.taleb@univ-chlef.dz Electrical Engineering Department, Hassiba Benbouali University, Laboratoire Génie Electrique et Energies Renouvelables (LGEER), BP 78C, Ouled Fares 02180, Chlef, Algeria

The Coefficient Diagram Method (CDM) is systematic that combines classical and modern control theories. Generally, it's used to design polynomial controllers where the degrees depend on the type of disturbance (steps, ramp, etc.) and the transfer function degree of the plant to define the Diophantine equation. Theoretically, the solution of this equation is difficult when the number of equations is great or less than that of unknowns. Compared to a pole placement method, the most important property of the CDM technique is that the calculation of the coefficients of the characteristic polynomial requires the system parameters, the controller parameters and the desired level of performance (stability index, settling time, etc.) [23]. In practice, the effectiveness of this approach has been demonstrated by much research recently published [17–19]. In microgrid systems, the CDM technique was applied by [24] and [25]. In [24], the authors present a distributed load frequency control method based on both the linear quadratic Gaussian (LQG) method and the CDM technique. In [25], a new application of robust virtual inertia control-based Coefficient Diagram Method controller is proposed. In this paper, PID controller gains are calculated according to the CDM technique to reduce the impact of frequency fluctuations of the microgrid system caused by a load demand and the connection of hybrid renewable energy sources. The basic idea of this method is to use the stability index and the equivalent time constant to compute the closed-loop characteristic polynomial of the overall system. The behaviour of the microgrid system based on the CDM-PID controller under different disturbances is investigated and compared with those of DE-PID and Chaotic PSO-PID control methods.

This paper is organized as follows: The theoretical background of the proposed method is presented in Section 1. A small signal model of the chosen configuration is given in Section 2. Section 3 resumes the steps to follow the design of the PID controller. The analysis of the obtained results is given in section 4. The paper ends with conclusions in Section 5.

2. Theoretical background: the coffecient diagram method

The block diagram of the CDM control system proposed by Manabe [24–31] is shown in Figure 1:
where

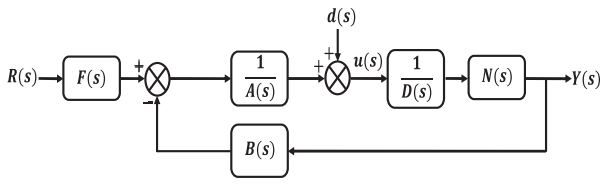

Figure 1. The standard bloc diagram of CDM.

$R(s)$ is the input signal reference, $Y(s)$ is the output signal, $u(s)$ is the controller signal and $d(s)$ is the external disturbance. $N(s)$ and $D(s)$ are the numerator and denominator polynomials of the controlled system, respectively, $F(s)$, $A(s)$ and $B(s)$ represent the polynomial controllers.

The closed-loop transfer function of the system is given by

$$Y(s) = \frac{N(s).F(s)}{P(s)}.R(s) + \frac{A(s).N(s)}{P(s)}.d(s) \tag{1}$$

where $P(s)$ is the polynomial characteristic of the system. Its coefficients are calculated by

$$P(s) = A(s).D(s) + B(s).N(s) \tag{2}$$

CDM is an indirect pole-placement method that aims to determine the convenient location for the closed-loop system's poles depending on the degree of the plant and the desired control performance: stability, settling time, etc [25–28]. In this case, the polynomials $A(s)$ and $B(s)$ of the CDM control structures are given as

$$A(s) = \sum_{i=0}^{p} l_i.s^i \tag{3}$$

$$B(s) = \sum_{i=0}^{q} k_i.s^i \tag{4}$$

where the condition $p \geq q$ must be satisfied for practical realization.

The coefficients of $P(s)$ are expressed in terms of k_i and l_i.

According to Manabe [23], the target characteristic polynomial is represented as in (5):

$$P(s) = \sum_{i=0}^{n} a_i.s^i \tag{5}$$

The stability index γ_i, the equivalent time constant τ and the stability limit γ_i^* are defined as

$$\gamma_i = \frac{a_i^2}{a_{i+1}.a_{i-1}}, i = 1, 2, \ldots.., n-1 \tag{6}$$

$$\gamma_n = \gamma_0 = \infty \tag{7}$$

$$\tau = \frac{a_1}{a_0} \tag{8}$$

$$\gamma_i^* = \frac{1}{\gamma_{i+1}} + \frac{1}{\gamma_{i-1}} \tag{9}$$

After defining the value of γ_i and τ, the target characteristic polynomial is derived in terms of a_0, τ and γ_i as [25–28]

$$P_t(s) = a_0.\left\{\left[\sum_{i=2}^{n}\left(\prod_{j=1}^{i-1}\frac{1}{\gamma_{i-j}^{j}}\right).(\tau.s)^i\right] + \tau.s + 1\right\} \tag{10}$$

By comparing each coefficient of characteristic equations between (2) and (10), the parameters of $A(s)$ and $B(s)$ polynomial controller are obtained. Generally, the recommended standard Manabe values of τ and γ_i are chosen as follows [32,33]:

$$\tau = \frac{t_s}{2.5 \sim 3} \tag{11}$$

where t_s is the user-specified settling time.

$$\gamma_i = [2.5, 2, \ldots\ldots, 2], \quad i = 1, 2, \ldots.., n-1 \tag{12}$$

The above values of γ_i can be changed to satisfy the desired performance.

$F(s)$ is obtained using the following expression [24–26]:

$$F(s) = \left.\frac{P(s)}{N(s)}\right|_{s=0} \tag{13}$$

The sufficient condition of stability is given as [25]

$$a_i > 1.12.\left[\frac{a_{i-1}}{a_{i+1}}.a_{i+2} + \frac{a_{i+1}}{a_{i-1}}.a_{i-2}\right] \tag{14}$$

$$\gamma_i > 1.12.\gamma_i^*, \quad i = 2, 3, \ldots., n-2 \tag{15}$$

3. Description of the hybrid power system with renewable generations

Microgrids are considered as a small-scale energy system with the integration of renewable sources and storage devices to supply a connected load demand which can be a critical load and commercial or industrial area that can be connected to the main grid or isolated in a remote area.

These renewable energy generations have random characteristics due to the environment and weather conditions change. The randomness in renewable energy sources and in load demands should be taken into account and requires the addition of storage devices such as battery energy storage systems (BESS), flywheel energy storage systems (FESS) and ultra-capacitor (UC) to improve the unbalance between load and generation. The diesel engine, microturbine and fuel cell are always integrated with the microgrid as supplementary sources to overcome the issues in the operation and stability of the microgrid. The different parts of a microgrid are connected through power converters. The proposed microgrid configuration is illustrated in Figure 2 [1], [3], [4], [7], [34]:

To study the stability of the system against external disturbances, we must present briefly the principle and the mathematical model of each element of the microgrid:

3.1. Photovoltaic system model

The photovoltaic solar module can capture the energy from the sun and convert it into a direct current. This phenomenon is based on the behaviour of semiconductor materials when they receive solar radiation. The generated power is changed according to solar radiation and environmental temperature. To analyze the frequency deviation behaviour in the frequency domain, it can be modelled by the first-order transfer function lag [1], [3], [4], [7]:

$$G_{STPG}(s) = \frac{\Delta P_{STPG}}{\Delta P_{Sol}} = \frac{K_S.K_T}{(1 + T_S.s).(1 + T_T.s)} \tag{16}$$

3.2. Model of the wind turbine generator

Wind turbines are mechanical devices which transform the wind force into electrical energy. These systems produce about 3% of the world's electricity. The performances of wind turbines depend on three parameters: the shape and length of the blades, the wind speed and

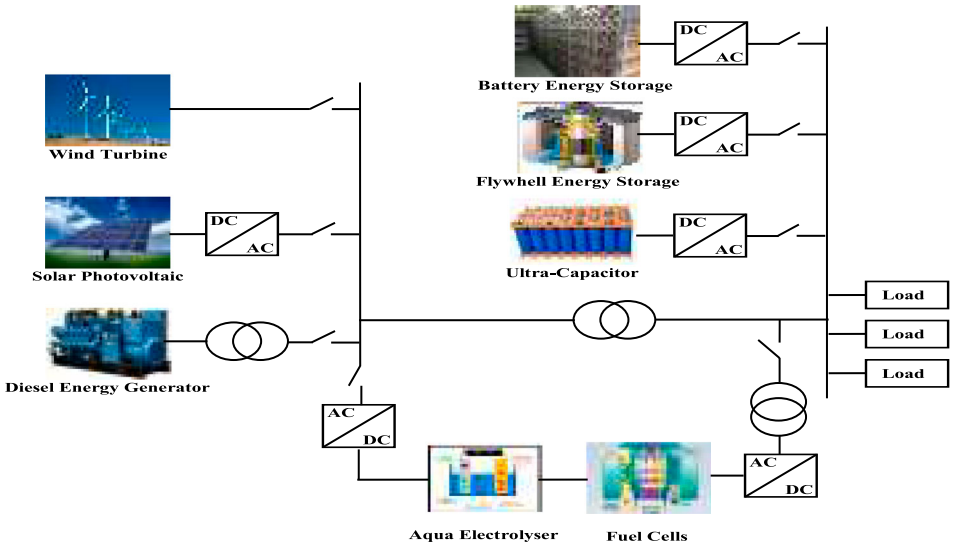

Figure 2. The simplified schematic model of the proposed microgrid.

finally the temperature. In this study for frequency analysis, the transfer function of wind turbine generator is given by first-order lag neglecting nonlinearities [1], [3], [4], [7]:

$$G_{WTG}(s) = \frac{\Delta P_{WTG}}{\Delta P_W} = \frac{K_{WTG}}{1 + T_{WTG}.s} \tag{17}$$

3.3. Fuel cell model

Fuel cells are static electrochemical devices that convert chemical energy into electrical energy through an electrochemical reaction. These generators utilize hydrogen as fuel and oxygen as the oxidant in the reaction to produce electricity, water and heat. In practice, the temperature released from this chemical reaction varies between 50°C and 1000°C. The simultaneous production of electricity and heat provides excellent energy efficiency. To analyze the frequency of the microgrid system, the fuel cell can be modelled by a transfer function in first-order [1], [3], [4], [7]:

$$G_{FC_{1,2}}(s) = \frac{\Delta P_{FC_{1,2}}}{\Delta P_{AE}} = \frac{K_{FC}}{1 + T_{FC}.s} \tag{18}$$

3.4. Diesel generator modelling

Diesel generators are electricity production systems consisting of a thermal generator and an alternator. This type of installation is often used as an emergency energy source in the event of the absence or failure of the public network. Sometimes, they use to supply isolated sites in the mountains or on the islands. They require speed regulation on the engine and voltage regulation on the alternator. In addition, they must be equipped with a set of sensors and safety devices. The diesel engine generator can be presented by a first-order transfer function [1], [3], [4], [7]:

$$G_{DEG}(s) = \frac{\Delta P_{DEG}}{\Delta u} = \frac{K_{DEG}}{1 + T_{DEG}.s} \tag{19}$$

3.5. Energy storage device models

In microgrid applications, energy storage batteries, ultra-capacitors and Flywheels are widely used to store the surplus of power from renewable sources to release it later when there is an imbalance between the demand and the generation. Generally, to study the stability of microgrid systems, these devices are modelled by first-order transfer functions [1], [3], [4], [7]:

$$G_{BESS}(s) = \frac{\Delta P_{BESS}}{\Delta u} = \frac{K_{BESS}}{1 + T_{BESS}.s} \tag{20}$$

$$G_{FESS}(s) = \frac{\Delta P_{FESS}}{\Delta u} = \frac{K_{FESS}}{1 + T_{FESS}.s} \tag{21}$$

$$G_{UC}(s) = \frac{\Delta P_{UC}}{\Delta u} = \frac{K_{UC}}{1 + T_{UC}.s} \tag{22}$$

3.6. Aqua electrolyzer

Aqua electrolyzer helps to decrease the rapid fluctuations in the microgrid system. It receives a part of the surplus power generated by wind and solar thermal systems to generate hydrogen based on the oxide reduction by the electrolyte. The generated hydrogen is used by the fuel cell as a foil. The aqua electrolyzer can be represented by a first-order transfer function as below [1] [3]:

$$G_{AE}(s) = \frac{K_{AE}}{1 + T_{AE}.s} = \frac{\Delta P_{AE}}{[(\Delta P_{WTG} + \Delta P_{STPG}).(1 - K_n)]} \tag{23}$$

The Aqua Electrolyzer uses the $(1 - K_n)$ fraction of the total power produced by WTG and STPG to produce hydrogen. In our application, K_n is 0.6.

3.7. Frequency deviation model

Microgrid systems must balance production and demand for power to ensure frequency and voltage stability. The integration of renewable energy sources affects the stability of microgrids, leads to an imbalance in the produced powers, and deviates the frequency from its nominal value. To maintain the system stable and less sensible to external disturbances, the frequency deviation (Δf) must be controlled. The power system model can be represented as follows [1], [3]:

$$G_{sys}(s) = \frac{\Delta f}{\Delta P_e} = \frac{1}{D + M.s} \tag{24}$$

where M and D are the equivalent inertia constant and damping constant, respectively.

All the components of the microgrid are modelled by the first transfer function with the associated parameters presented in Table 1 [1], [3]. The small signal model given in Figure 3 is considered to study the frequency stability of the microgrid against the climatic conditions and parametric variations [1], [3]:

The controller is inserted into the loop to control the frequency of the microgrid. It sends the control signal to

Table 1. Contains the result of comparing in pairs with the final result.

Microgrid components	Values
Wind Turbine Generator (WTG)	$T_{WTG} = 1.5, K_{WTG} = 1$
Aqua Electrolyzer (AE)	$T_{AE} = 0.5, K_{AE} = 0.002$
Fuel Cell (FC)	$T_{FC} = 4, K_{FC} = 0.01$
Flywheel Energy Storage System (FESS)	$T_{FESS} = 0.1, K_{FESS} = -0.01$
Battery Energy Storage System (BESS)	$T_{BESS} = 0.1, K_{BESS} = -0.003$
Ultra-Capacitor (UC)	$T_{UC} = 0.9, K_{UC} = -0.7$
Diesel Engine Generator (DEG)	$T_{DEG} = 2, K_{DEG} = 0.003$
Solar Thermal Power Generator (STPG)	$T_S = 1.8, K_S = 1.8, T_T = 0.3, K_T = 1$
Power System Model	$D = 0.3, M = 0.4$

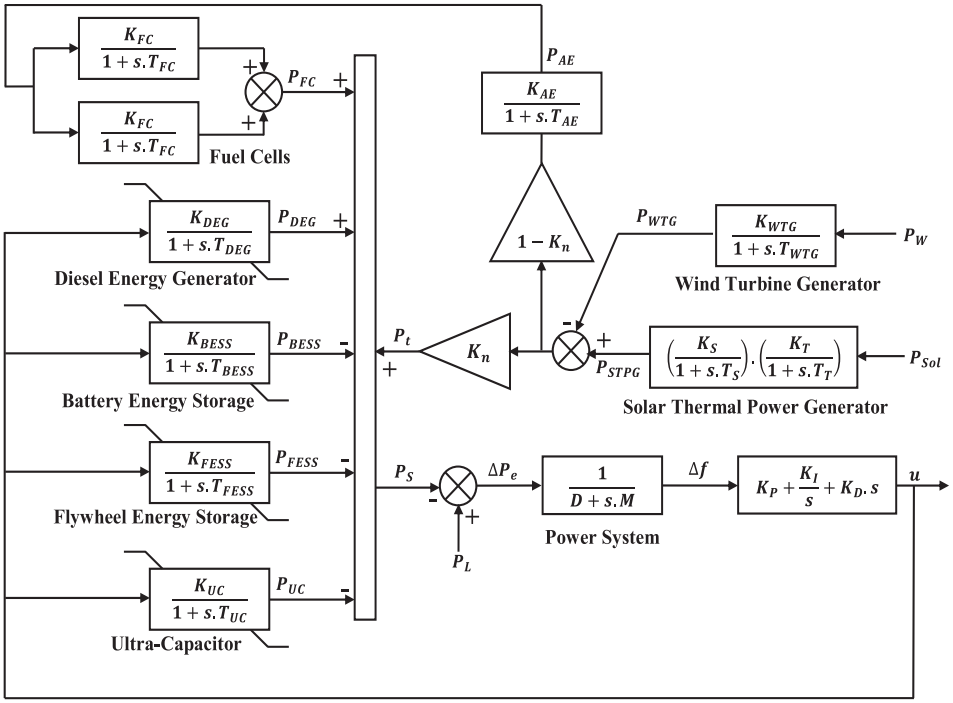

Figure 3. The small signal model of the proposed microgrid.

the storage systems to absorb/release additional/deficit power from/into the grid, respectively.

From the mathematical model we can write:

$$\Delta f = \frac{1}{D+M.s}.(P_L - P_{FC} - P_{DEG} + P_{FESS} + P_{BESS} + P_{UC}) \tag{25}$$

4. CDM-PID controller design for the proposed microgrid

To identify the parameters of the proposed controller used in this application by the CDM technique, the open-loop transfer function $G_0(s)$ of the system must be calculated. The microgrid system given in Figure 7 consists of four parallel blocks of controlled sources $G_{BESS}(s)$, $G_{FESS}(s)$, $G_{UC}(s)$ and $G_{DEG}(s)$ in series with the block $G_{sys}(s)$ of the power system. All other inputs change in the wind P_W, solar power P_S and the change in load demand P_L are acting as a disturbance input to the plant model. According to Table 1, the required open loop transfer function can be written as

$$G_0(s) = \frac{2.2736.(s+9.98).(s+8.743).(s+0.5013)}{(s+1.112).(s+0.4996).(s+0.07501).(s^2+19.99.s+100)} \tag{26}$$

This function has five poles: two of these are complexes. Theoretically, the location of poles in a complex plan can help us to understand the characteristics of the time response.

It's considered that there is a step disturbance affecting the system. According to Table 1 given in [23], the order of the polynomial controller must be4. In this work, we have chosen a second-order polynomial controller given by the following structure:

$$A(s) = l_2.s^2 + l_1.s + l_0, l_2 = l_0 = 0 \tag{27}$$

$$B(s) = k_2.s^2 + k_1.s + k_0 \tag{28}$$

where $\{k_2, k_1, k_0, l_1\}$ are the parameters to be set.

Compared to the conventional PID controller given by (28)

$$G_{PID}(s) = K_p + \frac{Ki}{s} + K_d.s \tag{29}$$

K_p, K_i and K_d can be identified as

$$K_p = \frac{k_1}{l1}, \quad K_i = \frac{k_0}{l1}, \quad K_d = \frac{k_2}{l1}$$

CDM is an algebraic approach combining classic and modern control theories and uses polynomial representation in a mathematical expression. According to the MG parameters given in Table 1, the characteristic polynomial of the closed-loop system can be expressed as follows:

$$P(s) = \sum_{i=0}^{n} a_i.s^i, \quad n = 6 \tag{30}$$

where

$$a_6 = 0.0072.l_1$$

$$a_5 = 0.01637.k_2 + 0.1561.l_1$$

$$a_4 = 0.3147.k_2 + 0.01637.k_1 + 0.9677.l_1$$

$$a_3 = 1.582.k_2 + 0.3147.k_1 + 0.01637.k_0 + 1.312.l_1$$

$$a_2 = 0.716.k_2 + 1.582.k_1 + 0.3147.k_0 + 0.493.l_1$$
$$a_1 = 0.716.k_1 + 1.582.k_0 + 0.03.l_1$$
$$a_0 = 0.716.k_0$$

This relationship highlights the stability of the closed-loop that depends on k_2, k_1, k_0 and l_1.

The design of the proposed controller by the CDM method requires knowledge of the values of the following parameters: the equivalent time constant τ and the stability indices, γ_1,γ_2, γ_3,γ_4, γ_5. In this case, the target characteristic polynomial in terms of τ and γ_i can be written as

$$P_t(s) = \sum_{i=0}^{n} at_i.s^i, \quad n = 6 \tag{31}$$

where

$$at_6 = a_0.\tau^6.\frac{1}{\gamma_5.\gamma_4^2.\gamma_3^3.\gamma_2^4.\gamma_1^5}$$
$$at_5 = a_0.\tau^5.\frac{1}{\gamma_4.\gamma_3^2.\gamma_2^3.\gamma_1^4}$$
$$at_4 = a_0.\tau^4.\frac{1}{\gamma_3.\gamma_2^2.\gamma_1^3}$$
$$at_3 = a_0.\tau^3.\frac{1}{\gamma_2.\gamma_1^2}$$
$$at_2 = a_0.\tau^2.\frac{1}{\gamma_1}$$
$$at_1 = a_0.\tau$$
$$at_0 = a_0$$

In the CDM technique, the Diophantine equation is obtained by equating the closed-loop system characteristic polynomial of (30) to the target polynomial characteristic given in (31). In Sylvester form, it's given by

$$[C]_{(n+1).(n+1)}.\begin{bmatrix} l_i \\ k_i \end{bmatrix} = [at_i]_{(n+1).1} \tag{32}$$

where n is the degree of the characteristic polynomial and $[C]$ is a square matrix of known values.

In our case, choosing a second-order polynomial controller brings us to a linear system (33) in which the number of equations 7 is greater than the number of unknowns 4. In mathematics, this system is overdetermined:

$$[C]_{7.4}.\begin{bmatrix} k_2 \\ k_1 \\ k_0 \\ l1 \end{bmatrix} = [at_i]_{7.1}, i = 0, 1, 2, \ldots 6 \tag{33}$$

where

$$[C]_{7x4} = \begin{pmatrix} 0 & 0 & 0 & 0.0072 \\ 0.0164 & 0 & 0 & 1.5820 \\ 0.3147 & 0.0164 & 0 & 0.9677 \\ 1.5820 & 0.3147 & 0.0164 & 1.3120 \\ 0.7160 & 1.5820 & 0.3147 & 0.4930 \\ 0 & 0.7160 & 1.5820 & 0.0300 \\ 0 & 0 & 0.7160 & 0 \end{pmatrix}$$

$$[at_i]_{7x1} = \begin{pmatrix} a_0.\tau^6.\frac{1}{\gamma_5.\gamma_4^2.\gamma_3^3.\gamma_2^4.\gamma_1^5} \\ a_0.\tau^5.\frac{1}{\gamma_4.\gamma_3^2.\gamma_2^3.\gamma_1^4} \\ a_0.\tau^4.\frac{1}{\gamma_3.\gamma_2^2.\gamma_1^3} \\ a_0.\tau^3.\frac{1}{\gamma_2.\gamma_1^2} \\ a_0.\tau^2.\frac{1}{\gamma_1} \\ a_0.\tau \\ a_0 \end{pmatrix}$$

The matrix $[C]$ has 7 rows (corresponding to equations) and 4 columns (corresponding to unknowns) and the vector $[at_i]$ has 7 rows. In general, there is no exact solution to this system. Then, the problem becomes how to identify a satisfactory solution to minimize a cost function. In practice, we can define a cost function as the square sum of errors to find the unknown vector. In this case, the solution given by the least squares method minimizes the square sum of error given by the following equation:

$$e(k_2, k_1, k_0, l_1) = [at_i]_{7x1} - [C]_{7.4}.\begin{bmatrix} k_2 \\ k_1 \\ k_0 \\ l1 \end{bmatrix}_2^2 \tag{34}$$

Expanding $e(k_2, k_1, k_0, l_1)$ gives:

$$e(k_2, k_1, k_0, l_1) = [at_i]^t.[at_i] - 2.[at_i].[C].\begin{bmatrix} k_2 \\ k_1 \\ k_0 \\ l1 \end{bmatrix} + \begin{bmatrix} k_2 \\ k_1 \\ k_0 \\ l1 \end{bmatrix}^t.[C]^t.[C].\begin{bmatrix} k_2 \\ k_1 \\ k_0 \\ l1 \end{bmatrix} \tag{35}$$

Taking the derivative gives:

$$\frac{\partial e}{\partial(k_2, k_1, k_0, l_1)} = -2.[C]^t.[at_i] + 2.[C]^t.[C].\begin{bmatrix} k_2 \\ k_1 \\ k_0 \\ l1 \end{bmatrix} \tag{36}$$

The minimum value for (34) is obtained when (k_2, k_1, k_0, l_1) satisfies:

$$\nabla\left(\frac{\partial e}{\partial(k_2, k_1, k_0, l_1)}\right) = 0 \tag{37}$$

The least-square solution is obtained by solving the linear system given by (33):

$$\begin{bmatrix} k_2 \\ k_1 \\ k_0 \\ l1 \end{bmatrix} = ([C]^t.[C])^{-1}.[C]^t.[at_i] \tag{38}$$

The matrix $([C]^t.[C])^{-1}.[C]^t$ is called the pseudo-inverse of $[C]$.

The CDM design procedure is summarized by the following flowchart (Figure 4):

In our application, the time constant τ and a_0 are chosen as

$$\tau = 2.8, \quad a_0 = 1$$

The stability indices γ_i are chosen as $\gamma_i = [2.5; 2; 2.2; 2; 2]$, $i = 1, \ldots, 5$, $\gamma_6 = \gamma_0 = \infty$. These parameters are chosen differently from the standard form of Manabe to decrease the frequency fluctuations of the microgrid.

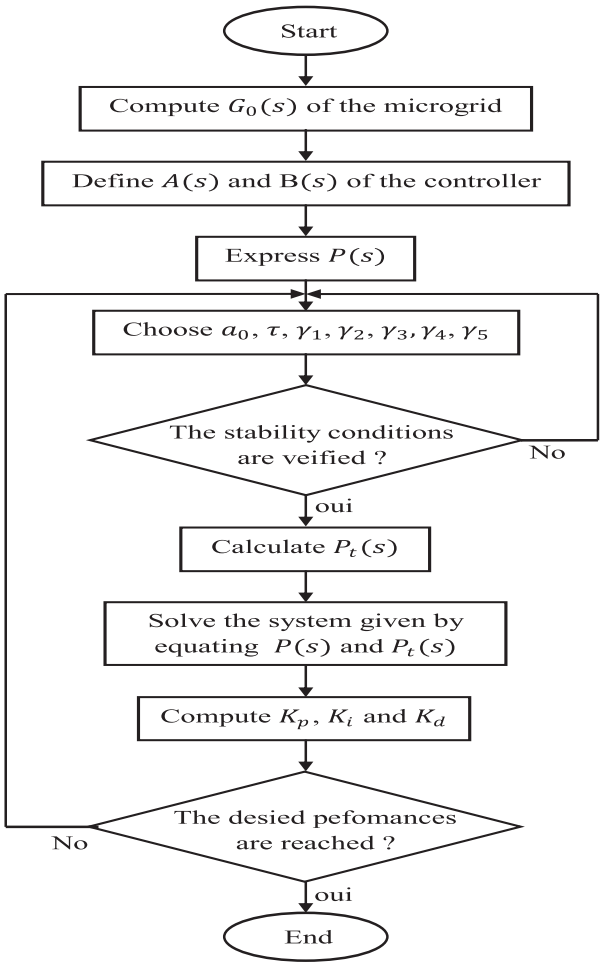

Figure 4. Simplified flowchart of the proposed technique.

The stability limits γ_i^* are calculated as

$$\gamma_i^* = [0.5; 0.8545; 1; 0.9545; 0.5], \quad i = 1, \ldots, 5 \tag{39}$$

The coefficients of the polynomial $P_t(s)$ become:

$$P_t(s) = 0.0036.s^6 + 0.0569.s^5 + 0.4470.s^4 + 1.7562.s^3 + 3.1360.s^2 + 2.8.s + 1 \tag{40}$$

Solving the system given by (32) gives the coefficients of the polynomial controller:

$$\boldsymbol{k_2} = 0.6571, \quad \boldsymbol{k_1} = 1.3557, \quad \boldsymbol{k_0} = 1.1974, \quad \boldsymbol{l_1} = 0.2194$$

Then, the parameters of the PID controller can be calculated as

$$\boldsymbol{K_p} = 6.1789, \quad \boldsymbol{K_i} = 5.4571, \quad \boldsymbol{K_d} = 2.9947$$

Figure 5 shows the coefficients of the characteristic polynomial and the stability indices chosen for the optimal synthesis of the PID controller. The coefficients a_i of the target characteristic polynomial on the vertical logarithmic scales are plotted against the number of power s on the horizontal linear scale. The chosen stability indices are compared to the Manabe standard form.

5. Simulation results and discussion

To demonstrate the effectiveness of the proposed tuning rule, the PID controller based on CDM algebraic technique is now tested by digital simulation using the microgrid model presented in Figure 2. By setting the simulation time to 120 s, the third-order Bogacki–Shampine method is used to integrate the studied closed-loop hybrid power system numerically. In this explicit method, the integration step is variable to guarantee that the error remains below a relative tolerance of 0.001. The mathematical model (40) is used to simulate the random fluctuations in the production of renewable energy sources (wind turbines, photovoltaic panels) and the energy demand of the connected loads [1]:

$$P = \left(\left(\emptyset.\eta.\sqrt{\beta}.[1 - G(s)] + \beta\right).\frac{\delta}{\beta}\right).\Gamma \tag{41}$$

where P represents the power output of the solar, wind or load model, $\emptyset$ is the stochastic component of the power, β contributes to the mean value of the power, $G(s)$ is a low-pass transfer function, $\{\eta, \delta\}$ are constants to normalize the generated or demand powers.

For wind power generation, the parameters of (41) are [1]

$$\emptyset \sim U(-1, 1),\ \eta = 0.8,\ \beta = 10,\ G(s) = \frac{1}{(1 + 10^4.s)},$$

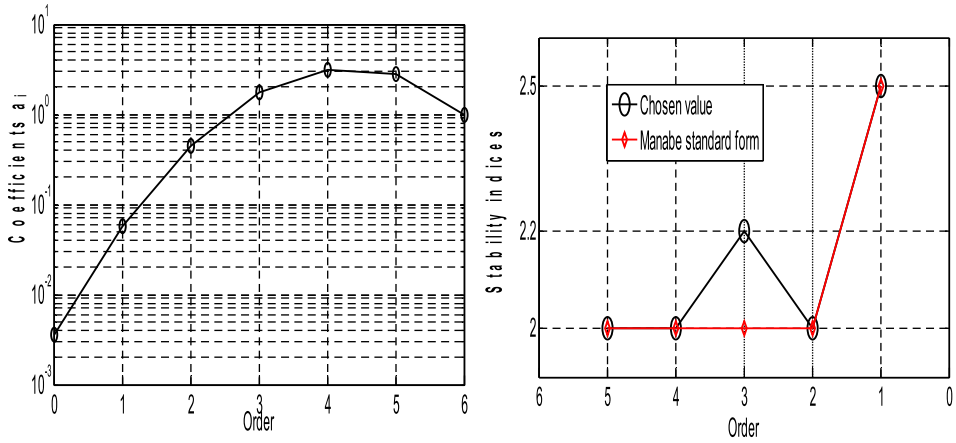

Figure 5. Simplified flowchart of the proposed technique.

$\delta = 1$ and $\Gamma = 0.5.\mathrm{H(t)} - 0.1.\mathrm{H(t-40)}$

For solar power generation, the parameters of (41) are [1]

$$\emptyset \sim U(-1,1),\ \eta = 0.7,\ \beta = 2,\ G(s) = \frac{1}{(1+10^4.s)},$$

$\delta = 0.1$ and $\Gamma = 1.1111.\mathrm{H(t)} - 0.5555.\mathrm{H(t-40)}$

For the load demand, the parameters of (41) are [1]

$$\emptyset \sim U(-1,1),\ \eta = 0.8,\ \beta = 100,$$
$$G(s) = \frac{300}{(1+300.s)} - \frac{1}{(1+1800.s)},$$

$\delta = 1$ and $\Gamma = \mathrm{H(t)} + 0.8.\mathrm{H(t-80)}$

Figure 6 represents the profiles of the powers of renewable energy sources and the power required by the load with the stochastic components:

The following two functions are used to evaluate the performances of the proposed design method [1]:

$$ISE = \int_0^{T_{max}} (\Delta f)^2 dt \tag{42}$$

$$ISDCO = \int_0^{T_{max}} (u - u_{ss})^2 dt \tag{43}$$

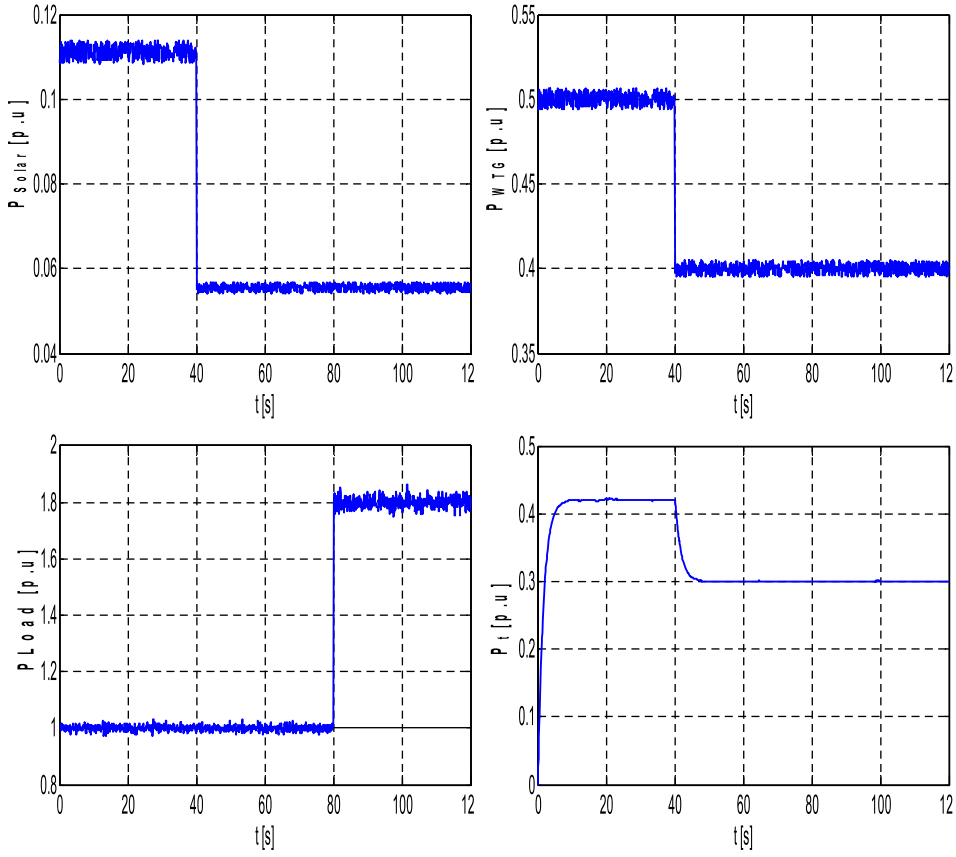

Figure 6. Power profiles of generation and load demand.

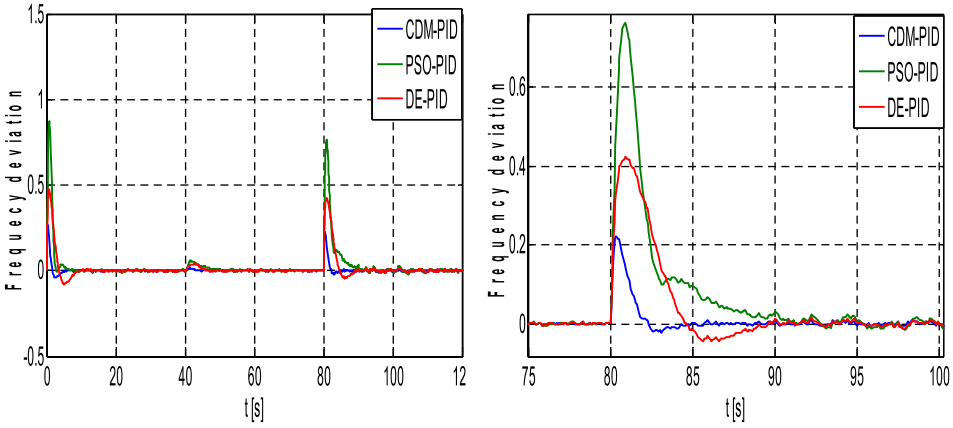

Figure 7. Frequency deviation of the microgrid system with different PID controllers.

Table 2. The results of comparing in pairs with the final result.

Method	K_p	K_i	K_d	Overshoot	*ISE*	*ISDCO*
PSO	2.04	0.64	0.61	76.3%	1.55	2.96
DE	1.8183	1.1829	1.7731	42.4%	0.683	2.737
CDM	6.1789	5.4571	2.9947	22.2%	0.084	6.874

for the present simulation study, $T_{\max} = 120s$ and $uss = 0.81H(t) + 0.17H(t-40) + 1.12H(t-80)$

The simulation is organized into three different scenarios.

Scenario 1: Performance of the hybrid power system under nominal operating conditions

To justify the use of the CDM technique, the performance properties of the designed PID controller are verified under nominal operating conditions of the hybrid power system. The variation in generated powers (P_{WTG}, P_{Solar}) and the demand power P_L given in Figure 6 are considered. The obtained results are compared with those of articles [1] and [3] where the parameters gains of the PID controller are optimized using the chaotic PSO algorithm and Differential Evolution Algorithm, respectively. The results of this comparison are given in Figure 7:

According to the simulation results, at $t = 80$, when the load power demand P_L increases from 1pu to 1.8pu, the frequency fluctuations are well damped with an overshoot of 22.2% for the system whose PID gains are calculated by the CDM approach, 42.4% for the DE algorithm and 76.3% the Chaotic PSO technique. Table 2 resumes the simulation results:

The PID controller, whose parameters are calculated by the CDM algorithm, gives better performance in terms of reduction in frequency fluctuations by 22.2% than the other algorithms. However, this reduction requires a relatively large control signal 6.874, which possibly presents a shock/stress on the mechanical parts of the controlled sources.

Scenario 2: The effects of stability indexes on system performance

To study the impact of the stability indices on the overall behaviour of the system and especially the frequency fluctuations under nominal operating conditions, a numerical simulation was carried out. In this case, the stability index γ_3 varied from 1.4 to 2.2; the results of the simulation performed with the profile of Figure 6 are represented in Figure 8 and Table 3.

Table 3. Measured performances against γ_3 variation.

γ_3	K_p	K_i	K_d	Overshoot	*ISE*	*ISDCO*
1.4	2.3423	2.0010	0.5831	56.2%	0.6741	2.155
1.8	3.7694	3.2868	1.4805	37%	0.2476	3.518
2.2	6.1789	5.4571	2.9947	22.2%	0.084	6.874

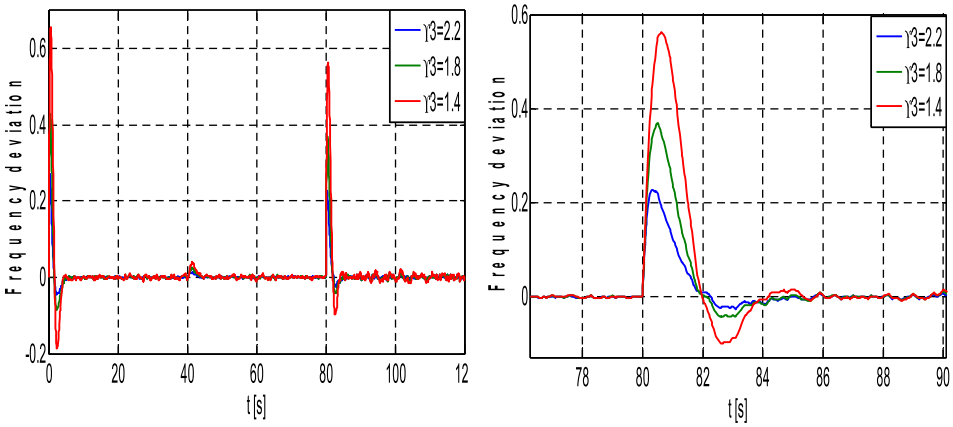

Figure 8. Frequency deviation against stability indice variation.

From these results, we note that the decrease in γ_3 leads to an increase in frequency fluctuations, which confirms that the judicious choice of stability indices plays a crucial role in the stability of the microgrid system.

Scenario 3: Robustness against ±10, ±30% and ±50% ultracapacitor parameter variations

Internal or external disturbances are undesirable events that can affect systems at any time. In microgrid applications, disturbances can be parametric or climatic variations. They can affect the stability of the overall system, which reduces energy efficiency or causes production discontinuity. To test the robustness of the closed-loop hybrid microgrid with the CDM-PID controller, a parametric variation of ±10, ±30% and ±50% was introduced in the ultracapacitor. The results of these tests are recorded in Figure 9 and tabulated in Table 4.

These results show that the CDM-based PID controller provides a good dynamic response against ±10, ±30% and ±50% parametric variations of ultracapacitor elements in comparison with the other controllers. The decrease in frequency fluctuations increases the stability of the microgrid system.

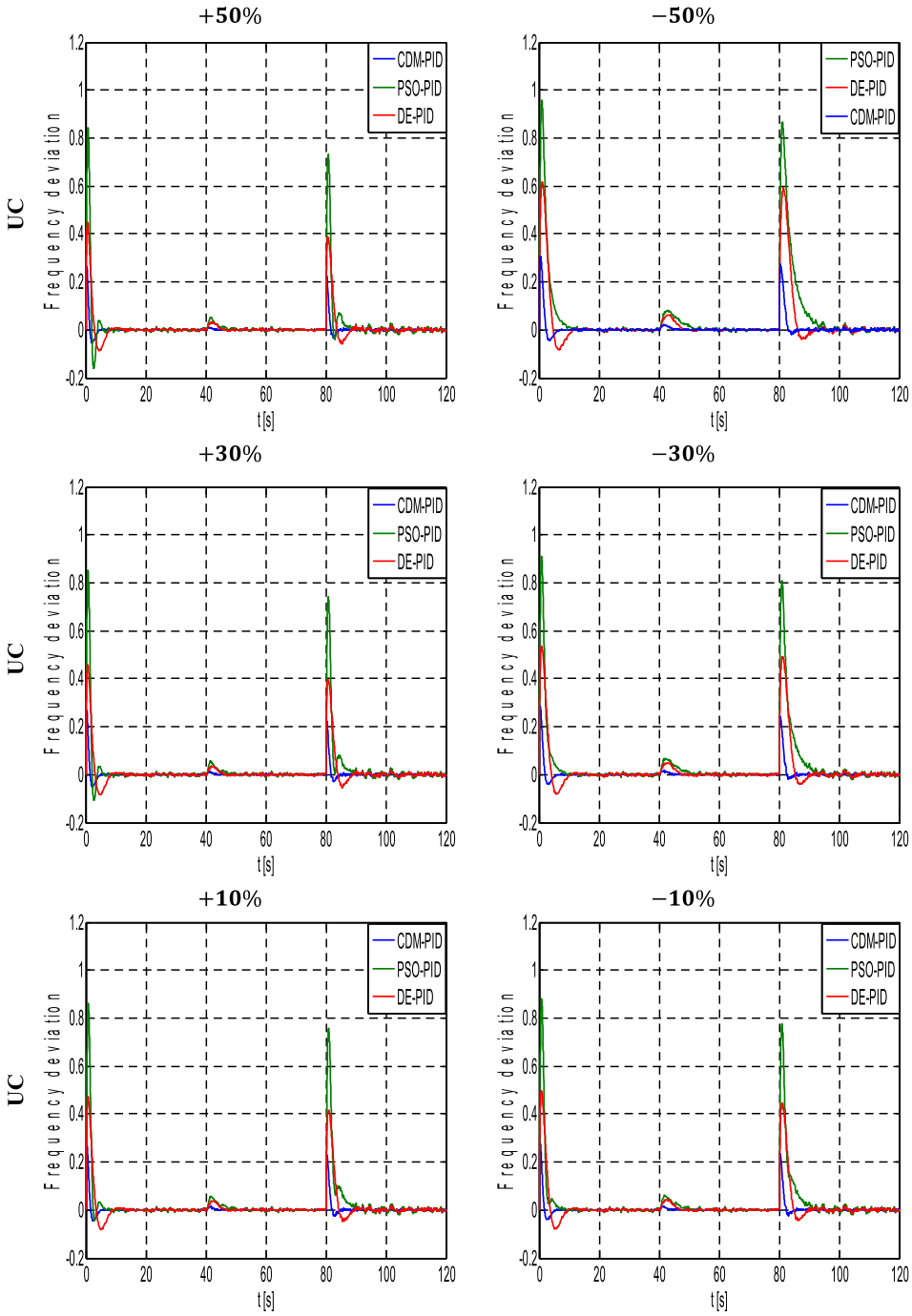

Figure 9. Frequency deviation against ±10, ±30% and ±50% parameter variations of UC.

Table 4. Robustness test against ±10, ±30% and ±50% parameter variations of UC.

		PSO		DE		CDM	
Controlled sources	Percentage	*ISE*	*ISDCO*	*ISE*	*ISDCO*	*ISE*	*ISDCO*
UC	+50%	1.14	26.71	0.479	27.88	0.072	32.49
	−50%	3.89	236.7	1.667	218.9	0.1789	229.3
	+30%	1.24	13.67	0.5383	14.61	0.0766	19.2
	−30%	2.37	49.09	1.067	43.93	0.1215	49.9
	+10%	1.443	3.041	0.6306	4.464	0.0838	9.112
	−10%	1.68	3.892	0.7844	5.63	0.0965	10.55

6. Conclusion

In this paper, an analytical approach is proposed to design a conventional PID controller to suppress the frequency fluctuations of a microgrid system under normal operating conditions and in the presence of disturbances. This technique known by the Coefficient Diagram Method is considered by the researchers as an indirect pole placement; its principle is based on the comparison of two characteristic polynomials of the same order; the coefficients of the first polynomial are calculated using the four unknown gains of the polynomial controller and the open-loop small signal model of the microgrid system. The coefficients of the desired closed-loop characteristic polynomial require the choice of the stability indices and the equivalent time constant. The resolution of the equation system resulting from this comparison gives the parameters of the PID controller. To test the advantage of the proposed technique by digital simulation, the designed PID controller is installed in the direct chain of the system and large parametric variations ±50% have been introduced in the ultracapacitor-controlled source to disturb the function of the microgrid. The obtained results are analyzed and compared to two previous works recently published where the PID controller is designed by DE and chaotic PSO algorithms, respectively. The reduced frequency oscillations in the presence of large parametric disturbances confirm the effectiveness of the proposed technique to design the PID controller.

Disclosure statement

No potential conflict of interest was reported by the author(s).

References

[1] Pan I, Das S. Fractional order fuzzy control of hybrid power system with renewable generation using chaotic PSO. ISA Trans. May 2016;62:19–29.
[2] Kumar B, Bhongade S. Load disturbance rejection based PID controller for frequency regulation of a microgrid. Indonesian J Electric Eng Comput Sci. September 2017;7:625–642.
[3] Pavan Kumar Neeli VSR, Salma U. Differential evolution algorithm based TID controller for autonomous hybrid power system. J Electric Eng. December 2018;12:15–23.
[4] Regad M, Helaimi M, Taleb R, et al. Fractional order PID control of hybrid power system with renewable generation using genetic algorithm. The 7th international conference on smart energy grid engineering (SEGE2019); IEEE;; 2019 Aug 12–14; Oshawa (ON).
[5] Pan I, Das S. Kriging based surrogate modeling for fractional order control of microgrids. IEEE Trans Smart Grid. Jan 2015;6:36–44.
[6] Alhamrouni I, Hairullah MA, Omar NS, et al. Modelling and design of PID controller for voltage control of AC hybrid micro-grid. Int J Power Electron Drive Syst (IJPEDS). March 2019;10:151–159.
[7] Regad M, Helaimi M, Taleb R, et al. Frequency control of microgrid with renewable generation using PID controller based Krill Herd. Indonesian J Electric Eng Inf (IJEEI). March 2020;8:21–32.
[8] Shayeghi H, Younesi A. Mini/micro-grid adaptive voltage and frequency stability enhancement using Q-learning mechanism through the offset of PID controller. J Oper Autom Power Eng. 2019;07:107–118.
[9] Koochakian Jazi M, Moghaddas Tafreshi SM, Jafari M. Design of a frequency control system in a microgrid containing HVAC. Turk J Electric Eng Comput Sci. 2016;24:2042–2052.
[10] Jena NK, Sahoo S, Nanda AB, et al. Frequency regulation in an islanded microgrid with optimal fractional order PID controller. Adv Intelligent Comput Commun. 2020;109:447–457.
[11] Balanagu P, Umavani M. A fuzzy-logic based control methodology in microgrids in the presence of renewable energy units". Int J Eng Technol. 2018;7:280–286.
[12] Asghar F, et al. Fuzzy logic-based intelligent frequency and voltage stability control system for standalone microgrid ". Int Trans Electric Energy Syst. 2017;28(4):1–14.
[13] Tamee K, Jandum K. Use of neural network model for frequency control in microgrid system. International symposium on multimedia and communication technology (ISMAC); Phranakhon Si Ayutthaya Rajabhat University; 2015 Sept 23–25; Ayutthaya.
[14] Akula SK, Salehfar H. Frequency control in microgrid communities using neural networks. North American power symposium (NAPS); IEEE; 2019 Oct 13–15; Wichita (KS).
[15] Sahu PC, Prusty RC, Panda S. Optimal design of a robust FO-multistage controller for the frequency awareness of an islanded AC microgrid under i-SCA algorithm. Int J Ambient Energy. 2020;43(1):1–13.
[16] Sahu PC, Prusty RC, Panda S. Frequency regulation of an electric vehicle-operated micro-grid under WOA-tuned fuzzy cascade controller. Int J Ambient Energy. 2020;43(1):1–12.
[17] Sahu PC, Prusty RC, Sahoo BK. Modified sine cosine algorithm-based fuzzy-aided PID controller for automatic generation control of multiarea power systems. Soft comput. 2020;24:12919–12936.
[18] Sahu PC, Mishra S, Prusty RC, et al. Improved-salp swarm optimized type-II fuzzy controller in load

frequency control of multi area islanded AC microgrid. Sustain Energy Grids Netw. 2018;16:380–392.
[19] Sahu PC, Baliarsingh R, Prusty RC, et al. Novel DQN optimised tilt fuzzy cascade controller for frequency stability of a tidal energy-based AC microgrid. Int J Ambient Energy. 2020;43(1):1–13.
[20] Sahu PC, Prusty RC, Panda S. Improved-GWO designed FO based type-II fuzzy controller for frequency awareness of an AC microgrid under plug in electric vehicle. Int J Ambient Energy. 2021;12: 1879–1896.
[21] Ali ES, Abd-Elazim SM. BFOA based design of PID controller for two area load frequency control with nonlinearities. Int J Electr Power Energy Syst. 2013;51:224–231.
[22] Ali ES, Abd-Elazim SM. Bacteria foraging optimization algorithm based load frequency controller for interconnected power system. Int J Electr Power Energy Syst. 2011;33:633–638.
[23] Giernacki W. A comparative analysis of tracking quality for CDM and PID control. 10th Portuguese conference on automatic control (CONTROLO'2012); 2012 July 16–18; Funchal.
[24] Mohamed TH, Zaki Diab AA, Hussein MM. Application of linear quadratic Gaussian and coefficient diagram techniques to distributed load frequency control of power systems. North American power symposium (NAPS), Vol. 5; 2015. pp. 1603–1615.
[25] Ali H, Magdy G, Li B, et al. A new frequency control strategy in an islanded microgrid using virtual inertia control-based coefficient diagram method. IEEE Access. 2019;7:16979–16990.
[26] Hanamoto T, Yamada H, Nashiren FM, et al. Controller design using coefficient diagram methods for matrix converter based unified power flow controllers. J Japan Soc Appl Electromagn Mech. 2013;21:369–374.
[27] Srisiriwat N, Wutthithanyawat C. Temperature control of autothermal reformer system with coefficient diagram method. IOP Conf Ser: Mater Sci Eng. 2017;241:1–5.
[28] Nyawat CW, Srisiriwat N. Temperature control of solid oxide fuel cell system with coefficient diagram method. Adv Eng Res. 2016;90:38–45.
[29] Maheswari C, Priyanka EB, Meenakshipriya B. Fractional-order $PI^{\lambda}D^{\mu}$ controller tuned by coefficient diagram method and particle swarm optimization algorithms for SO2 emission control process. Adv Eng Res. 2017;231:587–599.
[30] Erkan K, Can Yalçın B, Garip M. Three-axis gap clearance I-PD controller design based on coefficient diagram method for 4-pole hybrid electromagnet. Automatika. 2017;58:147–167.
[31] Amarnani D, Rajvant R, Thirunavukkarasu I, et al. Implementation of CDM based PID controller for a stable and double integrating process. J Mechatron Automation. 2015;2:15–22.
[32] Meenakshipriya B, Naveen C, Kalpana K. PSO tuning of a CDM based PID controller for ball and beam system. Int J Pure Appl Math. 2018;120:10905–10927.
[33] Fouad Haouari, Nourdine Bali, Mohamed Tadjine, et al. An observer for magnetic levitation system control based on a coefficient diagram method and backstepping. Arch Electr Eng. 2018;67:403–417.
[34] Jeya Veronica A, Senthil Kumar N. Load frequency controller design for microgrid using internal model control approach. Int J Renewable Energy Res. 2017;7(2): 778–786.
[35] Parameswaran S, Sharma R, Thondiyath A. Design and development of a depth controller for an autonomous underwater vehicle with variable buoyancy engine using coefficient diagram method. Proceedings of the 2018 2nd international conference on mechatronics systems and control engineering; 2018 Feb 21–23;, Amsterdam.